

Bayesian inferences of the thermal properties of a wall using temperature and heat flux measurements

Marco Iglesias^a, Zaid Sawlan^{b,*}, Marco Scavino^{b,d}, Raúl Tempone^b, Christopher Wood^c

^a*School of Mathematical Sciences, University of Nottingham, Nottingham, UK*

^b*King Abdullah University of Science and Technology, CEMSE, Thuwal, Saudi Arabia*

^c*Department of Architecture and Built Environment, University of Nottingham, Nottingham, UK*

^d*Instituto de Estadística (IESTA), Universidad de la República, Montevideo, Uruguay*

Abstract

We develop a hierarchical Bayesian inference method to estimate the thermal resistance and the volumetric heat capacity of a wall. These thermal properties are essential for accurate building energy simulations that are needed to make effective energy-saving policies. We apply our methodology to an experimental case study conducted in an environmental chamber, where measurements are recorded every minute from temperature probes and heat flux sensors placed on both sides of a solid brick wall over a five-day period. As a result of smoothing the measurements by local averaging procedure, we can reasonably assume that the temperature and the heat flux measurements have independent Gaussian noise. We model the heat transfer through the wall using the one-dimensional heat equation with unknown Dirichlet boundary conditions. We derive the joint likelihood of the wall parameters and the initial/boundary conditions. We then marginalize the nuisance boundary parameters from the joint likelihood. We obtain approximated Gaussian posterior distributions for the wall parameters and the initial temperature parameter. The results show that our technique reduces the bias error of the estimated wall parameters when compared to other approaches. Finally, we estimate the information gain under two experimental setups to recommend how the user can efficiently determine the duration of the measurement campaign and the range of the external temperature oscillation.

Keywords: Heat Equation, Nuisance Boundary Parameters Marginalization, Heat Flux Measurements, Solid Walls, Bayesian Inference, Thermal Resistance, Heat Capacity, Experimental Design.

2010 MSC: 35K20, 62F15, 62K05, 62P30, 80A20, 80A23.

1. Introduction

Concerns about climate change and the effects of greenhouse gases have led to international targets for reducing carbon emissions [1, 2]. One substantial source of carbon emissions is the built environment, which accounts for approximately one-third of global energy consumption [3]. For example, approximately 40% of national energy consumption in the UK is from the building sector. Reduction in carbon emissions from the built environment is therefore vital to meeting carbon reduction targets. Carbon emissions from buildings can be considerably reduced through large-scale policies that seek to limit energy demand for space heating and cooling [3]. Accurate predictions of building performance and energy demands are essential to the success of such policies. Specifically, computer simulations of heat loss from buildings are necessary to

*Corresponding author

Email addresses: marco.iglesias@nottingham.ac.uk (Marco Iglesias), zaid.sawlan@kaust.edu.sa (Zaid Sawlan), marco.scavino@kaust.edu.sa (Marco Scavino), raul.tempone@kaust.edu.sa (Raúl Tempone), christopher.wood@nottingham.ac.uk (Christopher Wood)

assess the effectiveness of energy-saving strategies such as retrofit interventions [4]. However, recent work [5, 6, 7] has shown that standard computer simulations of building performance may be unreliable due to inaccuracies from poorly characterized building structures including walls. Energy-saving measures based on inaccurate predictions of building performance may be economically ineffective.

Uncertainty in the thermal properties of walls is a primary source of inaccuracy in predictions of energy demand in buildings [7, 8]. The heat capacitance and thermal conductance (resistance) of walls are used in standard heat transfer models as parameters for building performance simulations. Since these parameters of existing buildings are often unknown, the corresponding inputs in building simulations are typically obtained by visual inspection and tabulated values. In most cases, these values do not provide accurate characterizations of the walls of the building under consideration.

1.1. Inferring thermal properties from in-situ measurements

The thermal properties of walls can be inferred from in-situ measurements of temperature and heat flux [9, 10, 7]. More specifically, the surface temperatures of internal and external walls denoted as $\{T_{int}^i\}_{i=1}^N$ and $\{T_{ext}^i\}_{i=1}^N$, are measured at a specified measurement location over time. In addition, the heat flux through the wall, $\{q^i\}_{i=1}^N$, is also measured at N equispaced time points. ISO 9869:2014 [11] outlines a simple averaging procedure to determine the thermal transmittance (U-value) from in-situ measurements. With this approach, the R-value (i.e., the inverse of the U-value) is computed directly by

$$R = \frac{\sum_{i=1}^N (T_{int}^i - T_{ext}^i)}{\sum_{i=1}^N q^i}.$$

Since the averaging procedure assumes that the thermal mass of the wall is zero or almost zero, the accuracy of the estimate of the U-value will require measurements collected over an extended period of time (often longer than two weeks) [9, 11]. More importantly, the averaging method does not provide a statistical framework that accounts for either the uncertainty in the thermal properties or errors in the measurements. As a result, this method fails to provide a proper quantification of the uncertainty in the estimated U-value of the wall.

Recent work has proposed the use of statistical approaches to infer thermal properties from in-situ measurements of temperature and heat flux with simplified heat transfer models. In particular, standard Bayesian inference has recently been proposed [9] to estimate the thermal properties of walls under the assumption that the heat dynamics of the wall can be described with a simple lumped-mass resistance-capacitance (RC) model. In contrast to the averaging method, the approach in [9] employs an RC network whose parameters include the thermal conductivity and the heat capacity. This standard Bayesian methodology suggests that these thermal properties can be inferred from in-situ measurements based on relatively shorter measurement campaigns than the ones required by the averaging method. While other non-Bayesian statistical methods for estimating thermal properties have been proposed [12], [9] provides substantial insight into the advantages of using Bayesian inference in building models and provides a motivation for further developments.

1.2. Our contribution

Inspired by [9], we develop a rigorous hierarchical Bayesian approach to inferring thermal properties of walls with realistic heat transfer models. We demonstrate how this methodology can be used for the optimal design of experiments to minimize the duration of measurement campaigns.

1.2.1. Description of the heat transfer by the heat equation

Most existing methodologies for inferring thermal properties [9] use forward models that can be derived from simplified coarse-grid approximations (often with 2 or 3 spatial nodes) of the heat equation that

describes heat transfer through a wall. These simplified models are often used for the sake of computational expediency in the parameter identification process. However, such simplifications introduce intrinsic modeling errors that may, in turn, result in biased and potentially inaccurate estimated parameters. In contrast, we use a heat equation with unknown Dirichlet boundary conditions to model the interior temperature of the wall and we provide a convergence analysis to assess the effect of the discretization error in the Bayesian estimates of the thermal properties. We show that the proposed technique is robust under grid refinement and is therefore suitable for any discretization that we may choose according to the computational resources at hand.

1.2.2. *Measurement errors in temperature measurements*

In-situ temperature measurements of a wall are often used as boundary conditions for a forward heat transfer model of the wall. In the Bayesian approach in [9] the inference of the thermal properties is made by inverting heat flux observations while using measurements of temperatures for the forward heat transfer model. Only the heat flux measurements are used to construct the likelihood function. Temperature measurements are assumed “exact” and are utilized as boundary conditions for the forward RC model in the Bayesian framework for inferring thermal properties. In contrast, our hierarchical approach uses a more accurate heat transfer model of the wall and also accounts for uncertainty in the temperature measurements. As we show in Section 3, failing to account for the uncertainty in these measurements can result in biased and inaccurate estimates of the inferred properties. To account for the uncertainty in temperature measurements, we develop a hierarchical Bayesian methodology in which we treat the nuisance boundary conditions as random functions modeled by Gaussian distributions. We provide the maximum likelihood estimate (MLE) and the posterior distributions of the unknown parameters, including the thermal properties. Under the specification of independent uniform density priors for the parameters of interest, we use the Laplace method and a Markov chain Monte Carlo (MCMC) algorithm to estimate their posterior distributions. We then compare our results with those obtained by applying a similar approach to the one in [9], in which smooth spline fits of the temperature measurements are used as exact boundary conditions.

1.2.3. *Experimental design*

Standard protocols based on asymptotic assumptions [11] require long measurement campaigns during winter to reduce the dynamic effect of the capacitance of the wall. In contrast, [9] suggests that shorter measurements campaigns may provide similar estimates of inferred parameters to the ones from longer measurement campaigns. Hence, we use the proposed hierarchical Bayesian framework to investigate the effects of the duration and the conditions (i.e., measurement cycle) of the measurement campaign. To this end, we estimate the information gain [13, 14] to quantify the duration of the measurement campaign and the corresponding cycle. The proposed approach can then be used to design cost-effective measurement campaigns.

The rest of this paper is organized as follows. In Section 2, we derive a simulation model of the heat flow process through a wall using the heat equation. Based on simple assumptions, we reduce the model to a one-dimensional heat equation with unknown Dirichlet boundary conditions. Then, we prove that the modeled heat flux can be written as a linear function of the boundary conditions. The Bayesian approach is then introduced; we construct the joint likelihood by assuming Gaussian noise in the heat flux measurements. We also assume that the nuisance boundary conditions are random functions modeled by Gaussian distributions. Under these assumptions, the marginalization of the boundary conditions can be performed analytically. Section 3 includes the description of the experiment conducted at the Nottingham University Innovation Park to collect temperature and heat flux measurements from both sides of a brick wall. Moreover, smoothing time series techniques are applied to the real data to assess the relevance of the measurement error. Example 1 shows how the thermal properties of the wall can be estimated when

a deterministic approximation of the nuisance boundary conditions is used. The numerical results of the marginalization technique are then presented in Example 2, where we also study the convergence of the ML estimates of the model parameters and estimate bivariate posterior distributions. In Subsection 3.5, we analyze the robustness of our Bayesian approach by means of bootstrap resampling methods. Finally, we compute the information gain about the model parameters under different experimental setups in Section 4.

2. Methodology

In this Section, we describe the forward and inverse methodologies used to characterize the thermal properties of walls. We also introduce the heat transfer (forward) model that we combine with the hierarchical Bayesian methodology introduced in Subsection 2.2.

2.1. The Forward model

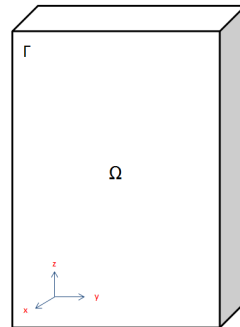
The existing forward models used to infer the thermal properties of walls are based on simplified heat transfer models [9]. Inferring parameters (i.e., thermal properties) from such simplified models can be done in a computationally affordable fashion through standard identification/inference techniques. However, as we stated earlier, this oversimplification of the heat transfer process might lead to modeling errors that are often not incorporated into standard inference approaches. In this Section, we propose a realistic mathematical model to simulate the heat transfer process through a wall using an initial/boundary value formulation for the heat equation.

2.1.1. Heat equation

The heat transport process inside a wall is modeled, in general, by a three-dimensional heat equation on a rectangular prism, Ω . The initial/boundary value problem for the heat equation along the period $[0, t_N]$, with initial wall temperature T_0 and temperature profile T_s at the boundary Γ , is given by:

$$\begin{aligned} \rho C \frac{\partial T}{\partial t} &= \nabla \cdot (k(\mathbf{x}) \nabla T), \mathbf{x} \in \Omega, t \in [0, t_N] \\ T(\mathbf{x}, t) &= T_s(\mathbf{x}, t), \mathbf{x} \in \Gamma, t \in [0, t_N] \\ T(\mathbf{x}, 0) &= T_0(\mathbf{x}), \mathbf{x} \in \Omega \end{aligned}$$

where ρ, C and k denote the density of the material, the heat capacity and the thermal conductivity, respectively.



Here, we consider the specific situation where the wall is surrounded by insulation materials and its thickness is less than its length and width. We therefore assume that the wall temperature varies only along the thickness dimension denoted by x . Also, given that the wall is solid, the thermal conductivity is assumed to be constant, $k(x) := k$. As a consequence, our simulation model consists of a one-dimensional heat equation with Dirichlet boundary conditions. From the solution of the heat equation, we then define the heat flux functions, F_{int} and F_{ext} , which correspond to the model predictions of heat fluxes at the

boundary. The model under consideration takes the following form:

$$\begin{cases} \rho C \frac{\partial T}{\partial t} = \frac{\partial}{\partial x} \left(k \frac{\partial T}{\partial x} \right), & x \in (0, L), t \in [0, t_N] \\ T(0, t) = T_{int}(t), T(L, t) = T_{ext}(t), & t \in [0, t_N] \\ T(x, 0) = T_0(x), & x \in (0, L), \\ F_{int}(t) = -k \frac{\partial T}{\partial x} \Big|_{x=0}, \\ F_{ext}(t) = -k \frac{\partial T}{\partial x} \Big|_{x=L}, \end{cases} \quad (1)$$

where L is the wall thickness, T_{int} and T_{ext} are the internal and external wall surface temperatures, respectively. In our implementation, we replace the thermal conductivity, k , with $\frac{L}{R}$ and estimate the thermal resistance, R , which is a property of the wall.

2.1.2. Numerical approximation

In the numerical implementation of the forward heat transfer model, it is relevant to show, upon discretization, that the heat flux can be written as a linear function of the initial condition, T_0 , and the boundary conditions, T_{int} and T_{ext} . This result is established in the following theorem whose proof is presented in the Appendix.

Theorem 2.1. *Consider the following uniform space-time discretization,*

$$\begin{aligned} x_0 = 0, x_1 = \Delta x, \dots, x_n = n\Delta x, \dots, x_M = M\Delta x = L, \\ t_0 = 0, t_1 = \Delta t, \dots, t_n = n\Delta t, \dots, t_N = N\Delta t, \end{aligned}$$

and define the vectors

$$\begin{aligned} \mathbf{T}_{int} &= (T_{int}(t_0), \dots, T_{int}(t_N))', \quad \mathbf{T}_{ext} = (T_{ext}(t_0), \dots, T_{ext}(t_N))', \\ \mathbf{T}_0 &= (T_0(x_1), \dots, T_0(x_{M-1}))', \\ \mathbf{F}_{int} &= (F_{int}(t_0), \dots, F_{int}(t_N))', \quad \mathbf{F}_{ext} = (F_{ext}(t_0), \dots, F_{ext}(t_N))'. \end{aligned}$$

Then, the discretized heat flux can be approximated by a linear function of the initial condition, \mathbf{T}_0 , and the boundary conditions, \mathbf{T}_{int} and \mathbf{T}_{ext} :

$$\mathbf{F}_{int} \approx H\mathbf{T}_0 + H_{int}\mathbf{T}_{int} + H_{ext}\mathbf{T}_{ext}, \quad (2)$$

$$\mathbf{F}_{ext} \approx G\mathbf{T}_0 + G_{int}\mathbf{T}_{int} + G_{ext}\mathbf{T}_{ext}, \quad (3)$$

where $H, H_{int}, H_{ext}, G, G_{int}$ and G_{ext} are matrices that may depend nonlinearly on the parameters R and ρC , which, in turn, we infer in the next Subsection. Such matrices are explicitly defined in the proof given in the Appendix.

Remark. *In the case in which thermal conductivity is not constant, Theorem 2.1 can be proved using the finite element method instead of the finite difference method (see [15]).*

In the subsequent analysis, we assume that the initial condition, $T_0(x)$ (and its corresponding discretization \mathbf{T}_0), is well approximated by the piecewise linear function

$$\begin{cases} T_{int}(0) + 2\frac{\tau_0 - T_{int}(0)}{L}x & \text{if } 0 < x \leq \frac{L}{2} \\ \tau_0 + 2\frac{T_{ext}(0) - \tau_0}{L}(x - \frac{L}{2}) & \text{if } \frac{L}{2} < x < L, \end{cases} \quad (4)$$

where τ_0 is an unknown constant parameter.

The discretized model (2)-(3) can be written as

$$\begin{bmatrix} \mathbf{F}_{int} \\ \mathbf{F}_{ext} \end{bmatrix} = \mathcal{F}(R, \rho C, \tau_0, \mathbf{T}_{int}, \mathbf{T}_{ext}), \quad (5)$$

where \mathcal{F} is a non-linear function that arises from the numerical discretization (2)-(3) and the modeling assumption (4).

2.2. The Bayesian inverse problem

Assume that we have noisy measurements of the heat fluxes, \mathbf{F}_{int} and \mathbf{F}_{ext} , at the observation times, t_0, \dots, t_N . We denote these measurements as $\mathbf{Q}_{int} = \{Q_{int}^0, \dots, Q_{int}^N\}$ and $\mathbf{Q}_{ext} = \{Q_{ext}^0, \dots, Q_{ext}^N\}$, respectively. Similarly, we assume that noisy measurements of the boundary temperatures, \mathbf{T}_{int} and \mathbf{T}_{ext} , are taken at those observation times. These observations are denoted by $\mathbf{Y}_{int} = \{Y_{int}^0, \dots, Y_{int}^N\}$ and $\mathbf{Y}_{ext} = \{Y_{ext}^0, \dots, Y_{ext}^N\}$, respectively. The objective of the proposed Bayesian methodology is to estimate $\theta = (R, \rho C, \tau_0)$ given heat flux measurements ($\mathbf{Q}_{int}, \mathbf{Q}_{ext}$) and boundary temperature measurements ($\mathbf{Y}_{int}, \mathbf{Y}_{ext}$). Whereas the parameters R and ρC are the unknown variables of interest that characterize the thermal properties of the wall, the initial temperature parameter, τ_0 , is also unknown. It must be inferred alongside R and ρC .

2.2.1. The Bayesian approach

We adopt the Bayesian approach in which the goal is to find the probability distribution of the unknown parameters, γ , given the data, namely the posterior distribution, $\rho(\gamma|data)$. From Bayes' theorem, the posterior distribution of γ is given by

$$\rho(\gamma|data) \propto \rho(data|\gamma)\rho_p(\gamma),$$

where $\rho(data|\gamma) = L(\gamma|data)$ is the likelihood function of γ and ρ_p is the prior distribution of γ [16]. In the context of the model defined by expression (5), we can see that the parameters of the model are $\theta \equiv (R, \rho C, \tau_0)$ as well as \mathbf{T}_{int} and \mathbf{T}_{ext} . Once these parameters are prescribed, expressions (2)-(3) determine the model predictions of the heat fluxes. Therefore, the joint posterior distribution of all these parameters is given by

$$\rho(\theta, \mathbf{T}_{int}, \mathbf{T}_{ext} | \mathbf{Q}_{int}, \mathbf{Q}_{ext}) \propto \rho(\mathbf{Q}_{int}, \mathbf{Q}_{ext} | \theta, \mathbf{T}_{int}, \mathbf{T}_{ext}) \rho_p(\theta, \mathbf{T}_{int}, \mathbf{T}_{ext}). \quad (6)$$

Note that θ is the unknown parameter of interest that contains the thermal properties of the wall.

In contrast, the boundary parameters, \mathbf{T}_{int} and \mathbf{T}_{ext} , are related to noisy measurements. Therefore, these nuisance boundary parameters will be marginalized from the joint likelihood. The specification of the prior distributions of these nuisance parameters is driven by the data by means of the boundary temperature measurements ($\mathbf{Y}_{int}, \mathbf{Y}_{ext}$). As a result, the joint likelihood function will be based only on the heat flux measurements. Nevertheless, by incorporating \mathbf{T}_{int} and \mathbf{T}_{ext} as unknown parameters in this hierarchical fashion, we are effectively taking into account the uncertainty in the corresponding temperature measurements ($\mathbf{Y}_{int}, \mathbf{Y}_{ext}$). This is a new contribution relative to [9] where the noise in these observations is neglected.

2.2.2. Joint likelihood

To construct the joint likelihood $\rho(\mathbf{Q}_{int}, \mathbf{Q}_{ext} | \theta, \mathbf{T}_{int}, \mathbf{T}_{ext})$, we assume that the heat flux measurements have Gaussian noise:

$$\begin{aligned} (\mathbf{Q}_{int} - \mathbf{F}_{int}) \Big|_{\{\theta, \mathbf{T}_{int}, \mathbf{T}_{ext}\}} &\sim N(\mathbf{0}, \Sigma_{int}), \\ (\mathbf{Q}_{ext} - \mathbf{F}_{ext}) \Big|_{\{\theta, \mathbf{T}_{int}, \mathbf{T}_{ext}\}} &\sim N(\mathbf{0}, \Sigma_{ext}). \end{aligned}$$

This assumption will be satisfied by the data used in the Bayesian analysis in Section 3.

Under the aforementioned assumption, the joint likelihood function of $\theta, \mathbf{T}_{int}, \mathbf{T}_{ext}$ is given by

$$\begin{aligned} L(\theta, \mathbf{T}_{int}, \mathbf{T}_{ext}, \Big|_{\mathbf{Q}_{int}, \mathbf{Q}_{ext}}) \\ = \frac{1}{(2\pi)^N \sqrt{|\Sigma_{int}| |\Sigma_{ext}|}} \exp \left\{ -\frac{1}{2} (\|\mathbf{Q}_{int} - \mathbf{F}_{int}\|_{\Sigma_{int}}^2 + \|\mathbf{Q}_{ext} - \mathbf{F}_{ext}\|_{\Sigma_{ext}}^2) \right\}. \end{aligned} \quad (7)$$

We emphasize that \mathbf{T}_{int} and \mathbf{T}_{ext} are nuisance parameters that appear in the formulation via the forward model (i.e., the heat equation). A direct approach to eliminating these parameters is to set $\mathbf{T}_{int} = \mathbf{Y}_{int}$ and $\mathbf{T}_{ext} = \mathbf{Y}_{ext}$ (recall that \mathbf{Y}_{int} and \mathbf{Y}_{ext} are measurements of the boundary temperatures). This approach is used in [9] where temperature measurements are considered to be deterministic boundary conditions of the RC model. Instead, we set $\mathbf{T}_{int} = \boldsymbol{\mu}_{int}$ and $\mathbf{T}_{ext} = \boldsymbol{\mu}_{ext}$ where $\boldsymbol{\mu}_{int}$ and $\boldsymbol{\mu}_{ext}$ are smoothed versions of \mathbf{Y}_{int} and \mathbf{Y}_{ext} , respectively. Moreover, rather than the simple RC model used in [9], here we consider a realistic model given by the heat equation introduced earlier. A rigorous approach to eliminate the aforementioned nuisance parameters is to marginalize them using data-driven priors [15]. This marginalization, which we conduct in the subsequent Subsection, enables us to account for the uncertainty in temperature measurements. As we demonstrate in Subsection 3.4, the marginalization process removes the bias in the inferred parameters, thereby providing accurate estimates and reliable quantification of their uncertainty.

2.3. Marginal likelihood

In this Section, we use temperature measurements to construct the data-driven Gaussian priors. We perform analytical integration to marginalize out the boundary conditions and obtain a marginal likelihood for θ . We assume independent Gaussian priors for the boundary conditions as follows:

$$\mathbf{T}_{int} \sim N(\boldsymbol{\mu}_{int}, C_{int,p}), \mathbf{T}_{ext} \sim N(\boldsymbol{\mu}_{ext}, C_{ext,p}), \quad (8)$$

where $\boldsymbol{\mu}_{int}$ and $\boldsymbol{\mu}_{ext}$ are smoothing splines constructed from the boundary temperature measurements. The exact expression of the marginal likelihood is provided in the following Theorem.

Theorem 2.2. *The marginal likelihood of θ is given by*

$$L(\theta | \mathbf{Q}_{int}, \mathbf{Q}_{ext}) \propto |\Lambda_0|^{1/2} |\Lambda_1|^{1/2} \exp \left\{ -\frac{1}{2} U + \frac{1}{2} t'_{int,2} \Lambda_0 t_{int,2} + \frac{1}{2} t'_{ext,1} \Lambda_1 t_{ext,1} \right\}, \quad (9)$$

where $\Lambda_0, \Lambda_1, U, t_{int,2}$ and $t_{ext,1}$ are independent of \mathbf{T}_{int} and \mathbf{T}_{ext} .

Proof. From equations (6),(7) and (8), the joint likelihood kernel of θ is given by

$$\begin{aligned}
& \exp \left\{ -\frac{1}{2} \left(\mathbf{Q}'_{int} \Sigma_{int}^{-1} \mathbf{Q}_{int} + (\mathbf{HT}_0)' \Sigma_{int}^{-1} (\mathbf{HT}_0) - 2\mathbf{Q}'_{int} \Sigma_{int}^{-1} (\mathbf{HT}_0) + \mathbf{Q}'_{ext} \Sigma_{ext}^{-1} \mathbf{Q}_{ext} + (\mathbf{GT}_0)' \Sigma_{ext}^{-1} (\mathbf{GT}_0) - 2\mathbf{Q}'_{ext} \Sigma_{ext}^{-1} (\mathbf{GT}_0) \right) \right. \\
& - \frac{1}{2} \left((H_{int} \mathbf{T}_{int})' \Sigma_{int}^{-1} (H_{int} \mathbf{T}_{int}) + 2(H_{int} \mathbf{T}_{int})' \Sigma_{int}^{-1} (\mathbf{HT}_0) + 2(H_{int} \mathbf{T}_{int})' \Sigma_{int}^{-1} (H_{ext} \mathbf{T}_{ext}) - 2\mathbf{Q}'_{int} \Sigma_{int}^{-1} (H_{int} \mathbf{T}_{int}) \right) \\
& - \frac{1}{2} \left((G_{int} \mathbf{T}_{int})' \Sigma_{ext}^{-1} (G_{int} \mathbf{T}_{int}) + 2(G_{int} \mathbf{T}_{int})' \Sigma_{ext}^{-1} (\mathbf{GT}_0) + 2(G_{int} \mathbf{T}_{int})' \Sigma_{ext}^{-1} (G_{ext} \mathbf{T}_{ext}) - 2\mathbf{Q}'_{ext} \Sigma_{ext}^{-1} (G_{int} \mathbf{T}_{int}) \right) \\
& - \frac{1}{2} \left((H_{ext} \mathbf{T}_{ext})' \Sigma_{int}^{-1} (H_{ext} \mathbf{T}_{ext}) + 2(H_{ext} \mathbf{T}_{ext})' \Sigma_{int}^{-1} (\mathbf{HT}_0) - 2\mathbf{Q}'_{int} \Sigma_{int}^{-1} (H_{ext} \mathbf{T}_{ext}) \right) \\
& - \frac{1}{2} \left((G_{ext} \mathbf{T}_{ext})' \Sigma_{ext}^{-1} (G_{ext} \mathbf{T}_{ext}) + 2(G_{ext} \mathbf{T}_{ext})' \Sigma_{ext}^{-1} (\mathbf{GT}_0) - 2\mathbf{Q}'_{ext} \Sigma_{ext}^{-1} (G_{ext} \mathbf{T}_{ext}) \right) \\
& \left. - \frac{1}{2} \left(\boldsymbol{\mu}'_{int} C_{int,p}^{-1} \boldsymbol{\mu}_{int} - 2\boldsymbol{\mu}'_{int} C_{int,p}^{-1} \mathbf{T}_{int} + \mathbf{T}'_{int} C_{int,p}^{-1} \mathbf{T}_{int} + \boldsymbol{\mu}'_{ext} C_{ext,p}^{-1} \boldsymbol{\mu}_{ext} - 2\boldsymbol{\mu}'_{ext} C_{ext,p}^{-1} \mathbf{T}_{ext} + \mathbf{T}'_{ext} C_{ext,p}^{-1} \mathbf{T}_{ext} \right) \right\}, .
\end{aligned}$$

Let U include any term that is independent from \mathbf{T}_{int} and \mathbf{T}_{ext} ; that is:

$$\begin{aligned}
U = & \mathbf{Q}'_{int} \Sigma_{int}^{-1} \mathbf{Q}_{int} + \mathbf{Q}'_{ext} \Sigma_{ext}^{-1} \mathbf{Q}_{ext} + (\mathbf{HT}_0)' \Sigma_{int}^{-1} (\mathbf{HT}_0) + (\mathbf{GT}_0)' \Sigma_{ext}^{-1} (\mathbf{GT}_0) \\
& - 2\mathbf{Q}'_{int} \Sigma_{int}^{-1} (\mathbf{HT}_0) - 2\mathbf{Q}'_{ext} \Sigma_{ext}^{-1} (\mathbf{GT}_0) + \boldsymbol{\mu}'_{int} C_{int,p}^{-1} \boldsymbol{\mu}_{int} + \boldsymbol{\mu}'_{ext} C_{ext,p}^{-1} \boldsymbol{\mu}_{ext} .
\end{aligned}$$

Define

$$\begin{aligned}
t'_{int,1} = & [\mathbf{Q}'_{int} - (\mathbf{HT}_0)' - (H_{ext} \mathbf{T}_{ext})'] \Sigma_{int}^{-1} H_{int} + [\mathbf{Q}'_{ext} - (\mathbf{GT}_0)' - (G_{ext} \mathbf{T}_{ext})'] \Sigma_{ext}^{-1} G_{int} + \boldsymbol{\mu}'_{int} C_{int,p}^{-1}, \\
\Lambda_0 = & \left(H'_{int} \Sigma_{int}^{-1} H_{int} + G'_{int} \Sigma_{ext}^{-1} G_{int} + C_{int,p}^{-1} \right)^{-1} .
\end{aligned}$$

By integrating first with respect to \mathbf{T}_{int} , the marginal likelihood of θ and \mathbf{T}_{ext} is proportional to the product of a factor that is independent of \mathbf{T}_{int} and the term $(2\pi)^{N/2} |\Lambda_0|^{1/2} \exp \left\{ \frac{1}{2} t'_{int,1} \Lambda_0 t_{int,1} \right\}$.

Now, let

$$\begin{aligned}
t'_{int,2} = & (\mathbf{Q}'_{int} - (\mathbf{HT}_0)') \Sigma_{int}^{-1} H_{int} + (\mathbf{Q}'_{ext} - (\mathbf{GT}_0)') \Sigma_{ext}^{-1} G_{int} + \boldsymbol{\mu}'_{int} C_{int,p}^{-1}, \\
\Lambda_1^{-1} = & H'_{ext} \Sigma_{int}^{-1} H_{ext} + G'_{ext} \Sigma_{ext}^{-1} G_{ext} + C_{ext,p}^{-1} - (H'_{ext} \Sigma_{int}^{-1} H_{int} + G'_{ext} \Sigma_{ext}^{-1} G_{int}) \Lambda_0 (H'_{int} \Sigma_{int}^{-1} H_{ext} + G'_{int} \Sigma_{ext}^{-1} G_{ext}) \\
t'_{ext,1} = & (\mathbf{Q}'_{int} - (\mathbf{HT}_0)') \Sigma_{int}^{-1} H_{ext} + (\mathbf{Q}'_{ext} - (\mathbf{GT}_0)') \Sigma_{ext}^{-1} G_{ext} + \boldsymbol{\mu}'_{ext} C_{ext,p}^{-1} - t'_{int,2} \Lambda_0 (H'_{int} \Sigma_{int}^{-1} H_{ext} + G'_{int} \Sigma_{ext}^{-1} G_{ext}).
\end{aligned}$$

By integrating with respect to \mathbf{T}_{ext} , the marginal likelihood of θ is proportional to the product of a factor that is independent of \mathbf{T}_{ext} and the term $(2\pi)^{N/2} |\Lambda_1|^{1/2} \exp \left\{ \frac{1}{2} t'_{ext,1} \Lambda_1 t_{ext,1} \right\}$. \square

The marginal likelihood (9) can now be used in the Bayesian framework, summarized in Subsection 2.2.1, to compute the posterior distribution, $\rho(\theta | \mathbf{Q}_{int}, \mathbf{Q}_{ext})$.

3. Experimental data and numerical results

In this Section, we apply the proposed Bayesian approach to infer the thermal properties of a wall from in-situ measurements of heat flux and temperature collected under controlled conditions. In Subsection 3.1, we describe the experimental setup. The results from the Bayesian analysis are presented in Subsections 3.3 and 3.4.

3.1. Experimental setup

Data were collected from an experiment conducted inside an environmental chamber in the Energy Technologies Building, Nottingham University Innovation Park. The chamber consisted of two rooms separated by a 215–mm thick partition wall. The two rooms had internal dimensions of $3.70 \times 3.50 \times 2.38$

m. The data were collected from a $970 \times 600 \times 215$ -mm brick section of the partition wall. Heat flux sensors and temperature probes were placed on both sides of the bricks. According to CIBSE Guide A [17] (Tables 3.38, 3.47), reference values of R and ρC for the wall under consideration should be in the range of $[0.279, 0.3846]$ (m^2K/W) and $[3.01 \times 10^5, 3.76 \times 10^5]$ (J/m^2K), respectively. The temperature in Room 2 fluctuated based on hourly weather data collected from Nottingham city during 8 to 15 February 2014.

Figure 1 shows the temperature and heat flux time series, both consisting of 6,900 measurements recorded every minute. Clearly, these raw measurements are contaminated by unknown noise. To analyze this noise, we use a smoothing spline method to fit a curve to each time series. This approach is based on the reasonable assumption that the real temperature and heat flux, according to the characteristics of the conducted experiment, vary smoothly over time. The noise is then approximated by the difference between the raw measurements and the smooth values.

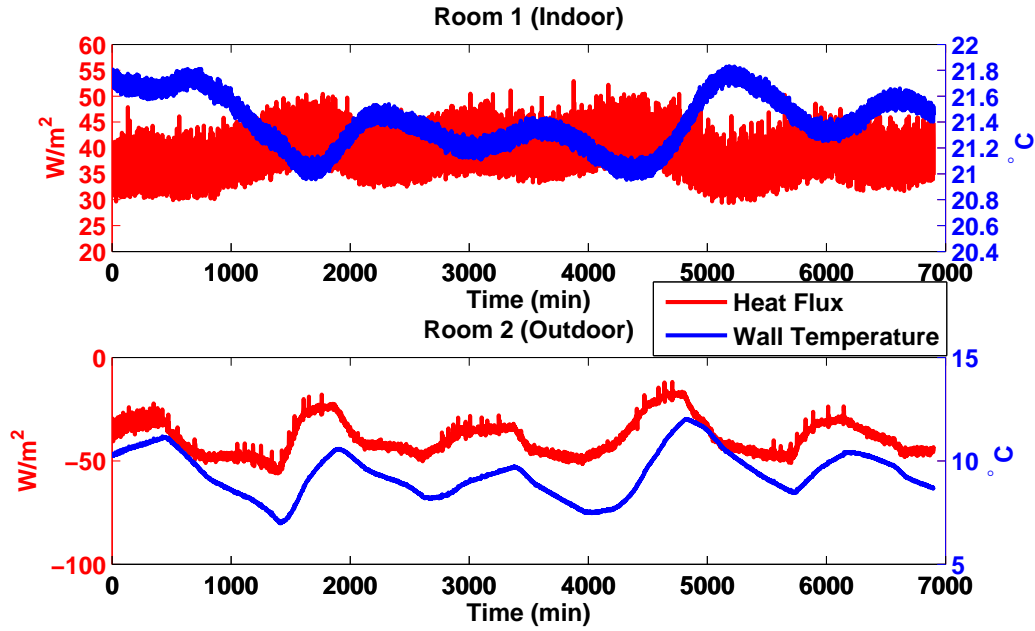


Figure 1: Raw temperature and heat flux measurements. Temperature in Room 2 imitates outdoor weather conditions.

3.2. Smoothing the data

We assume that the time series $\mathbf{y} = (y_1, \dots, y_N)$ follows the regression model

$$y_i = g(t_i) + \epsilon_i, \quad i = 1, \dots, N,$$

where $g(\cdot)$ is a smooth function that belongs to

$$W_2^{(m)} = \{f : f^{(j)} \text{ is absolutely continuous, } j = 0, 1, \dots, m-1, \text{ and } f^{(m)} \text{ is square integrable}\}$$

and that ϵ_i are independent Gaussian random variables with zero mean and unknown variance, σ^2 . We estimate g by fitting a function to $\mathbf{y} = (y_1, \dots, y_N)$ and adding a penalty measure of roughness:

$$\min_{f \in W_2^{(m)}} \frac{1}{N} \sum_{i=1}^N (f(t_i) - y_i)^2 + \lambda \int (f^{(m)}(u))^2 du,$$

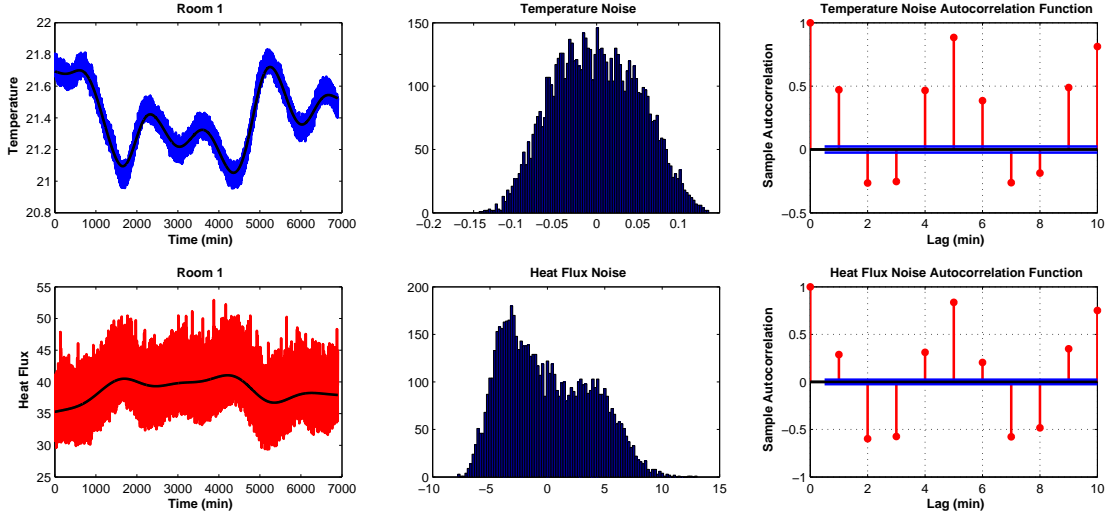


Figure 2: Estimated noise of the raw temperature and heat flux measurements in Room 1.

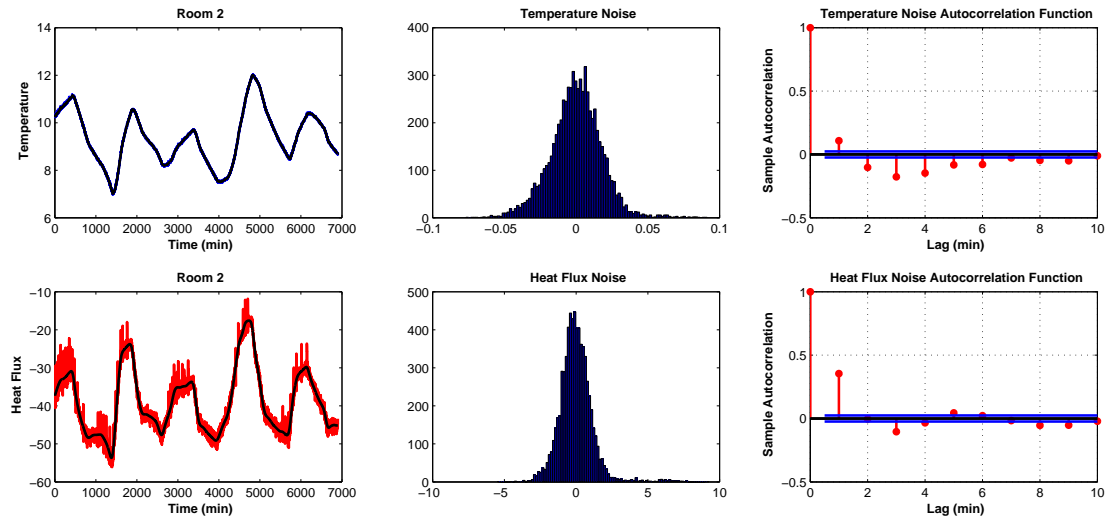


Figure 3: Estimated noise of the raw temperature and heat flux measurements in Room 2.

where λ is the smoothing parameter. Several methods choose the smoothing parameter, λ (see, for example, [18, 19]). Here, we consider a cubic smoothing spline estimator for g where $m = 2$, which is computed by a MATLAB function (CSAPS). We choose λ to minimize the autocorrelation function of the estimated noise.

Figures 2 and 3 shows the estimated noise of the raw temperature and heat flux measurements on both sides of the wall. We notice that the estimated noise, especially in Room 1, is not Gaussian. Also, the autocorrelation function of the noise shows strong correlations, requiring the estimation of dense covariance matrices. We therefore consider a moving average of the raw data by computing local averages for every five consecutive measurements, where 5 is the lag of the moving average. We choose the lag to minimize the autocorrelation functions of the noise for the four time series simultaneously. Figures 4 and 5 shows the estimated noise of the moving average temperature and heat flux, where we can see that the estimated

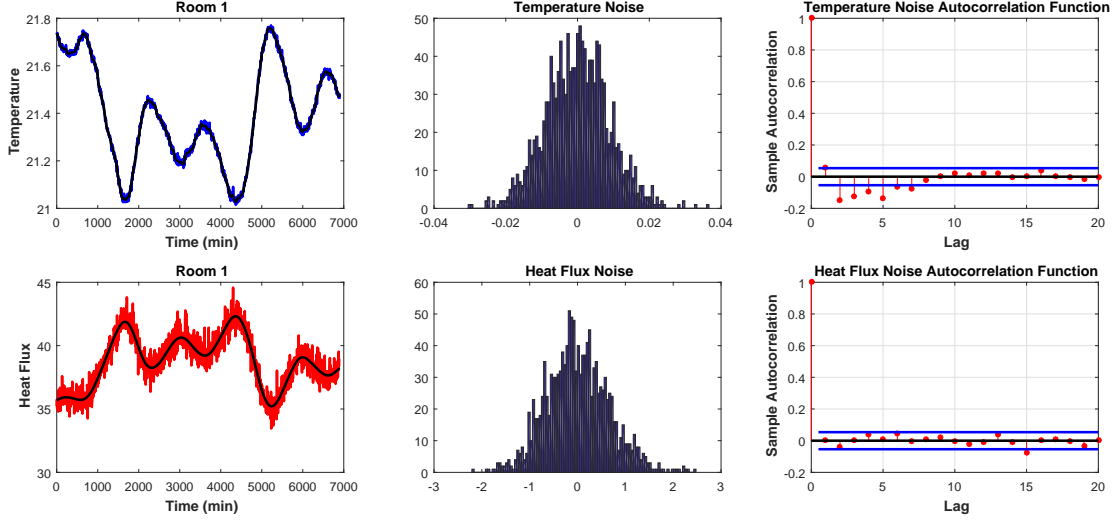


Figure 4: Estimated noise of the moving average temperature and heat flux in Room 1.

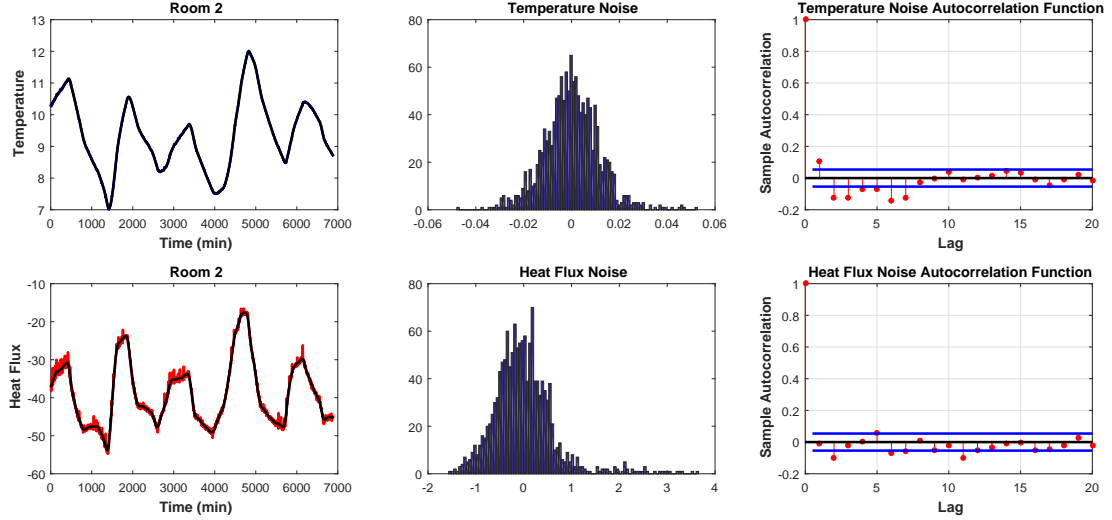


Figure 5: Estimated noise of the moving average temperature and heat flux in Room 2.

noise looks Gaussian for all the time series. Moreover, the corresponding autocorrelations are considerably reduced. We replace the raw measurements shown in Figure 1 with the moving average series and henceforth refer to these series as the data.

3.3. Numerical Example 1

In this Subsection, we report a numerical example in which we use the Bayesian framework to infer the thermal properties of the wall by following a direct approach similar to the one in [9] in which the boundary conditions, \mathbf{T}_{int} and \mathbf{T}_{ext} , are assumed to be exact. However, in contrast to [9] in which raw measurements are used, here \mathbf{T}_{int} and \mathbf{T}_{ext} are approximated by smoothing splines constructed from the boundary temperature measurements. The moving average heat fluxes, \mathbf{Q}_{int} and \mathbf{Q}_{ext} , are assumed to be Gaussian distributed and uncorrelated. Moreover, $\Sigma_{int} = \sigma_{int}^2 \mathcal{I}$, $\Sigma_{ext} = \sigma_{ext}^2 \mathcal{I}$, where $\sigma_{int} = \sigma_{ext} = 0.66$,

which is the empirical standard deviation of the two moving average heat flux series. In this example, to get a likelihood function of θ , we modify the joint likelihood (7) by removing the dependency of \mathbf{T}_{int} and \mathbf{T}_{ext} , which are assumed to be known. In other words, the likelihood is given by

$$L(\theta|\mathbf{Q}_{int}, \mathbf{Q}_{ext}) = \frac{1}{(2\pi\sigma_{int}\sigma_{ext})^N} \exp \left\{ - \left(\frac{1}{2\sigma_{int}^2} \|\mathbf{Q}_{int} - \mathbf{F}_{int}\|_2^2 + \frac{1}{2\sigma_{ext}^2} \|\mathbf{Q}_{ext} - \mathbf{F}_{ext}\|_2^2 \right) \right\}. \quad (10)$$

We maximize the likelihood function using a MATLAB function (FMINUNC) with several initial guess points. In the optimization algorithm, the heat equation is solved using $M = 60$ in the space mesh for each time step, $\Delta t = 60$ seconds. The heat flux functions are computed by equations (14)-(15) for every five time steps. Then, the maximum likelihood (ML) estimates of the model parameters are

$$R = 0.3107, \rho C = 3.17 \times 10^5, \tau_0 = 16.11.$$

Note that the values of R and ρC are well within the range provided by the tabulated values as described at the beginning of this section. We also assess the consistency of such ML estimates by plugging them into the forward model to compare the simulated heat flux with the experimental measurements. Figures 6 and 7 show that the heat flux simulations, computed by using the above ML estimates of θ , are consistent with the data.

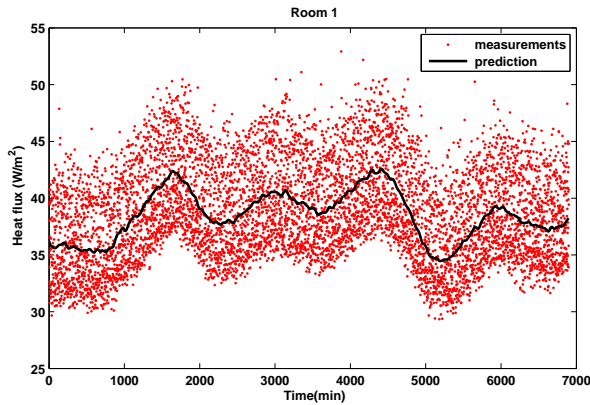


Figure 6: Raw heat flux measurements (red dots) with a model prediction for Room 1.

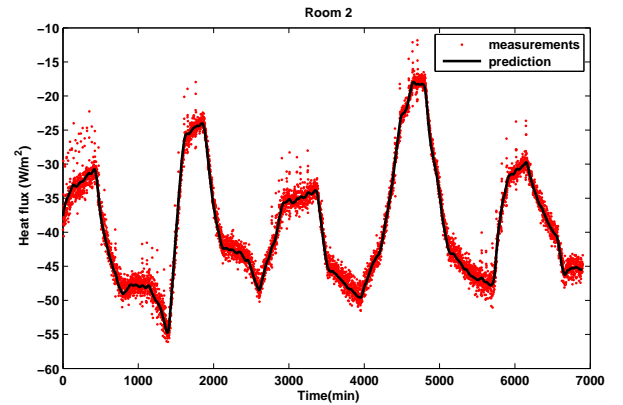


Figure 7: Raw heat flux raw measurements (red dots) with a model prediction for Room 2.

We now take the Bayesian approach by computing the posterior distribution of θ associated with the likelihood (10):

$$\rho(\theta|\mathbf{Q}_{int}, \mathbf{Q}_{ext}) \propto L(\theta|\mathbf{Q}_{int}, \mathbf{Q}_{ext})\rho_p(\theta).$$

To specify the joint prior, $\rho_p(\theta) = \rho_p(R, \rho C, \tau_0)$, we assume independence among the parameters and we consider the following uniform priors:

$$R \sim U(0.17, 0.36), \rho C \sim U(234000, 431000), \tau_0 \sim U(5, 25).$$

The marginal posterior densities of R , ρC and τ_0 are obtained by using the Laplace method and a Markov chain Monte Carlo (MCMC) sampling algorithm. The Laplace method provides a Gaussian ap-

proximation of the posterior distribution of θ as follows:

$$\rho(\theta|\mathbf{Q}_{int}, \mathbf{Q}_{ext}) \approx \frac{1}{\sqrt{2\pi|H(\hat{\theta})|}} \exp \left\{ -(\theta - \hat{\theta})^{tr} H(\hat{\theta})^{-1} (\theta - \hat{\theta}) \right\},$$

where $\hat{\theta}$ is the maximum a posteriori (MAP) probability estimate of θ and $H(\hat{\theta})$ is the Hessian matrix of the log posterior evaluated at $\hat{\theta}$ [20, Chapter 4].

We used the random-walk Metropolis-Hastings algorithm (1) to generate MCMC samples (see [21, Chapter 6]). We ran the MCMC chain 101,000 times, with a 1,000-iteration burn-in period and every twentieth draw of the chain kept. Figure 8 shows that the Laplace method provides a very accurate approximation of the three posterior densities when compared with the simulation-based posterior densities. The marginal posterior densities of R and τ_0 are highly concentrated around their respective modes.

Algorithm 1 Random-walk Metropolis-Hastings algorithm

- 1: **set** an initial value for the chain: $\theta_c = \theta_0$ and **choose** the covariance $diag(\delta)$
 - 2: **run** the forward model at θ_c up to time t_N
 - 3: **compute** $a = \text{loglikelihood}(\theta_c) + \text{logprior}(\theta_c)$
 - 4: **draw** θ_p from $N(\theta_c, diag(\delta))$
 - 5: **run** the forward model at θ_p up to time t_N
 - 6: **compute** $b = \text{loglikelihood}(\theta_p) + \text{logprior}(\theta_p)$
 - 7: **let** $H = \min(1, \exp(b - a))$ and **draw** r from $U(0, 1)$
 - 8: **if** $H > r$ **then**
 - 9: $\theta_c = \theta_p$
 - 10: $a = b$
 - 11: **repeat** steps (2 to 10) **until** L posterior samples are obtained.
-

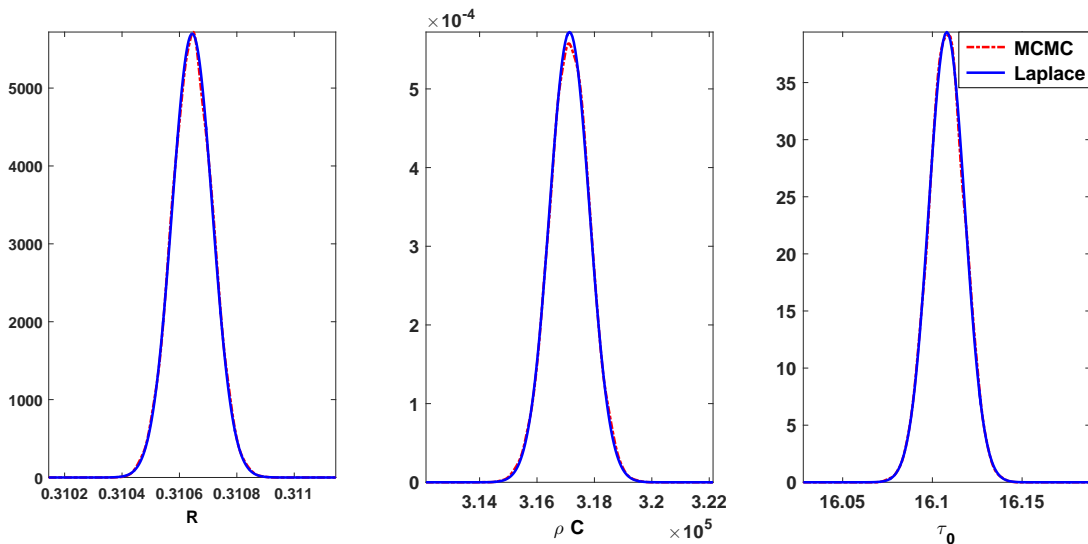


Figure 8: Marginal posteriors of the model parameters R , ρC and τ_0 approximated by the Laplace method (blue line) and the random-walk Metropolis-Hastings algorithm (red line).

3.4. Numerical Example 2

In this example, we incorporate uncertainty in the observations of \mathbf{T}_{int} and \mathbf{T}_{ext} and we apply our proposed hierarchical approach to characterize the posterior distribution of θ that arises from the marginalized likelihood (9). More precisely, we assume that the nuisance boundary conditions, \mathbf{T}_{int} and \mathbf{T}_{ext} , are modeled by the Gaussian distributions introduced in (8), where $\boldsymbol{\mu}_{int}$ and $\boldsymbol{\mu}_{ext}$ are the smoothing splines constructed from the boundary temperature data and $C_{int,p} = C_{ext,p} = (0.01)^2 \mathcal{I}$. Similar to Example 3.3, the moving averages, \mathbf{Q}_{int} and \mathbf{Q}_{ext} , for heat flux are assumed to be Gaussian distributed and uncorrelated with $\Sigma_{int} = \Sigma_{ext} = (0.66)^2 \mathcal{I}$.

The ML estimates of the components of θ corresponding to the marginal likelihood (9) are

$$R = 0.3106, \rho C = 3.20 \times 10^5, \tau_0 = 16.11.$$

Given the ML estimates, we plot the predicted median heat flux with 95% confidence bands in Figures 9 and 10, where the boundary conditions are sampled from

$$\mathbf{T}_{int} \sim N(\boldsymbol{\mu}_{int}, (0.01)^2 \mathcal{I}), \quad \mathbf{T}_{ext} \sim N(\boldsymbol{\mu}_{ext}, (0.01)^2 \mathcal{I}).$$

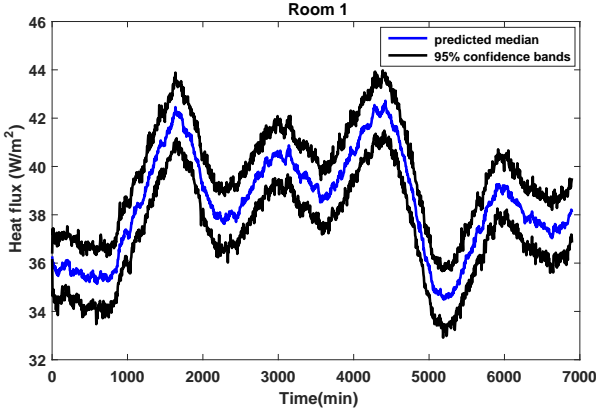


Figure 9: Median prediction (blue line) and 95% confidence bands (black lines) for the heat flux in Room 1.

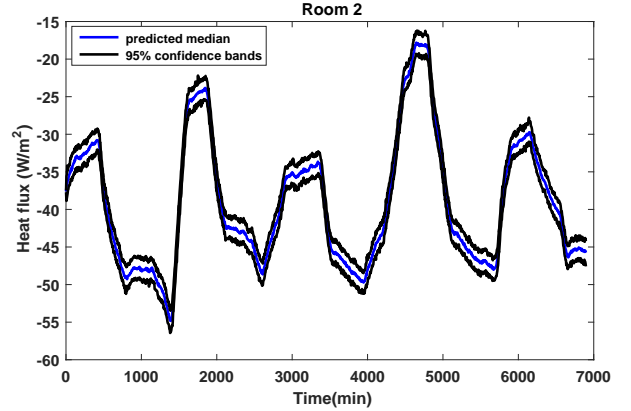


Figure 10: Median prediction (blue line) and 95% confidence bands (black lines) for the heat flux in Room 2.

One of the main contributions of our work, relative to existing Bayesian approaches that infer the thermal properties of walls, is that we use the heat equation to describe heat transfer through the wall. Analysis of the effect of the space-time discretization ($\Delta x, \Delta t$) on ML estimates of the components of θ is therefore necessary. We determined that the convergence of the ML estimates is quadratic with respect to Δx and linear with respect to Δt as shown in Figures 11 and 12, respectively.

We now consider the Bayesian approach using the marginal likelihood defined in (9) with the following uniform priors:

$$R \sim U(0.17, 0.36), \rho C \sim U(234000, 431000), \tau_0 \sim U(5, 25).$$

We again obtain the corresponding marginal posterior densities by the Markov chain Monte Carlo (MCMC) sampling algorithm (Algorithm 1) and by using the Laplace method. Figure 13 shows the estimated marginal posteriors for R , ρC and τ_0 . The Laplace method and the MCMC technique provide very similar estimated marginal posterior densities. Also, Figures 14 and 15 show the correlation between the thermal resistance, R , and the volumetric heat capacity, ρC . In Figure 16, we compare these marginal posteriors with the ones obtained in Subsection 3.3 where the boundary parameters are assumed to be determinis-

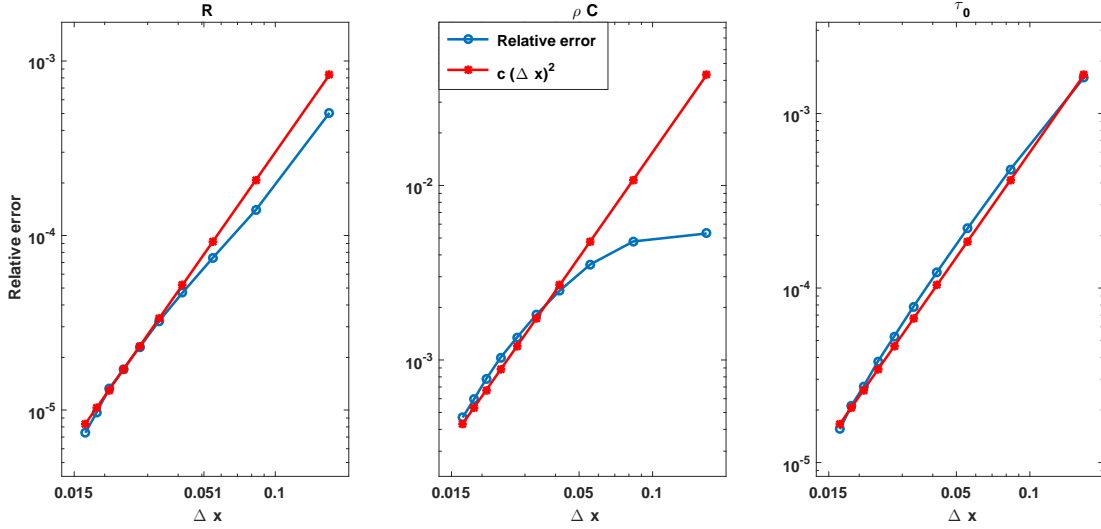


Figure 11: Convergence analysis of ML estimates with respect to Δx .

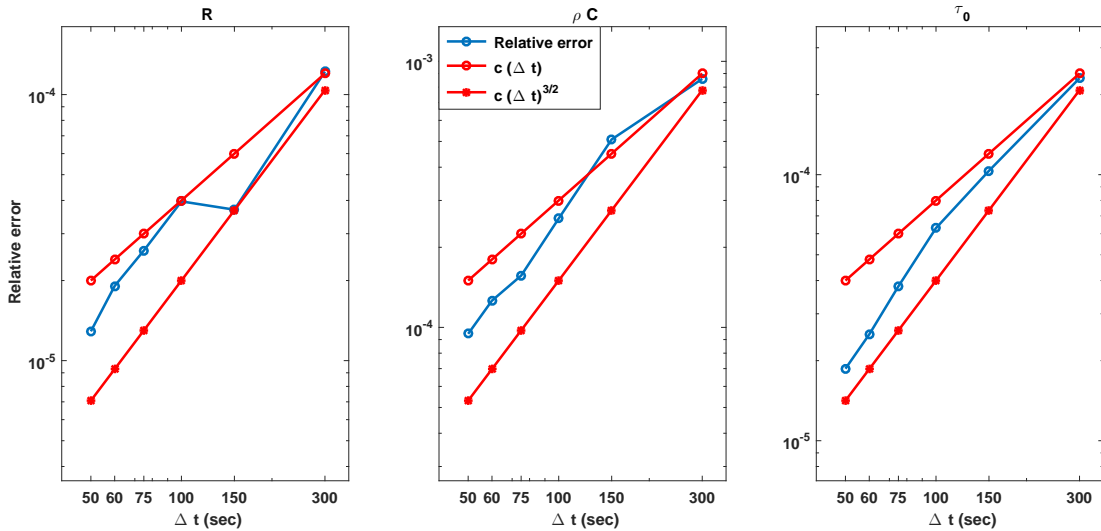


Figure 12: Convergence analysis of ML estimates with respect to Δt .

tic. The direct deterministic approach provides over-concentrated posteriors and relatively biased MAP estimates. On the other hand, the marginalization approach incorporates uncertainties into the nuisance boundary parameters, thereby producing realistic posterior densities.

3.5. Robustness analysis

To assess the robustness of our Bayesian approach, we consider a subsampling method that generates variability intervals for R and ρC . First, the raw time series are divided into consecutive, non-overlapping subintervals of length ℓ . Then, we resample the original time series in which subsamples of size b are drawn from each subinterval. The local average is computed for each subsample to filter the sampled time series. We use smoothing splines to model the boundary temperature parameters. We then use our Bayesian approach under the same uniform priors used in Examples 3.3 and 3.4. By repeating this procedure, we

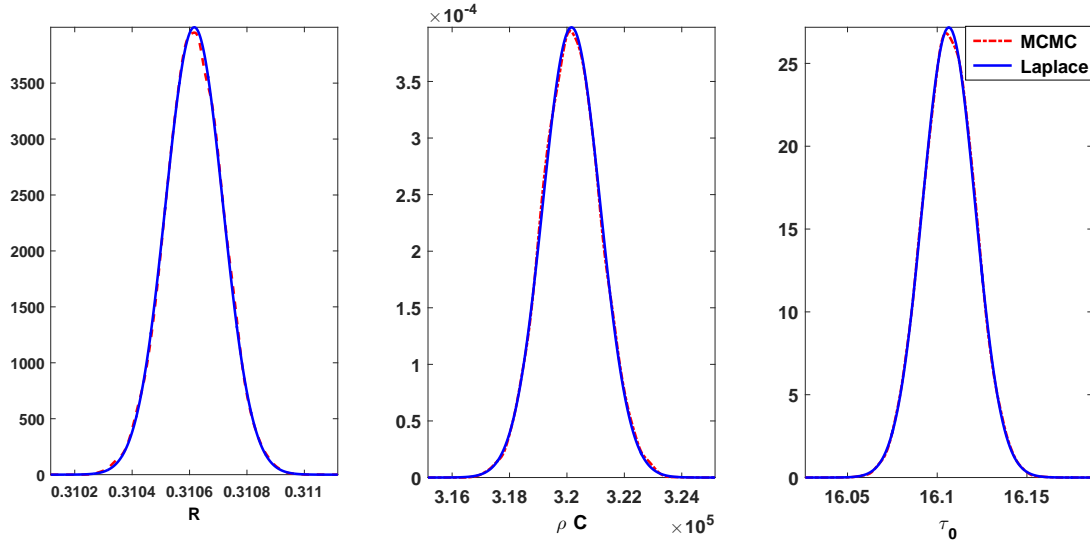


Figure 13: Marginal posteriors of R , ρC and τ_0 approximated by the Laplace method (blue line) and the random-walk Metropolis-Hastings algorithm (red line).

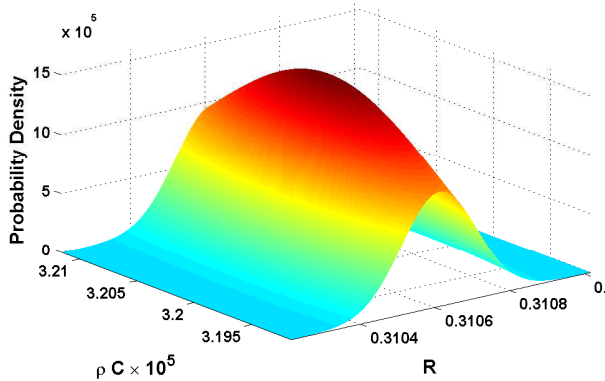


Figure 14: Approximated bivariate posterior distribution of R and ρC .

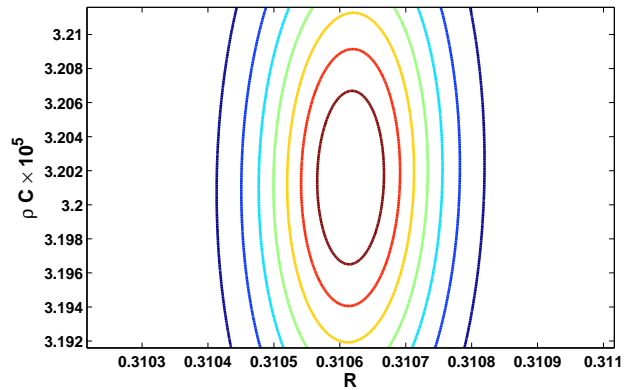


Figure 15: Contour plot of the approximated bivariate posterior distribution of R and ρC .

obtain several MAP estimates. We summarize the variability of these estimates by means of boxplots. The subsampling procedure is summarized in Algorithm 2.

Algorithm 2 Subsampling algorithm

- 1: **partition** the raw time series into subintervals D_i , $i = 1, \dots, \ell$
 - 2: **sample** b observations from each D_i without replacement
 - 3: **compute** local averages for each subsample
 - 4: **estimate** μ_{int} and μ_{ext} using smoothing spline fit of the averaged time series
 - 5: **apply** the Bayesian inference given the averaged heat flux measurements
 - 6: **repeat** steps (2 to 4) **until** L MAP estimates are obtained.
-

Figures 17 and 18 show the variability intervals obtained for R and ρC using the subsampling algorithm that draws b observations randomly from each subinterval of size ℓ . In Figure 17, we use $\ell = 5$ and

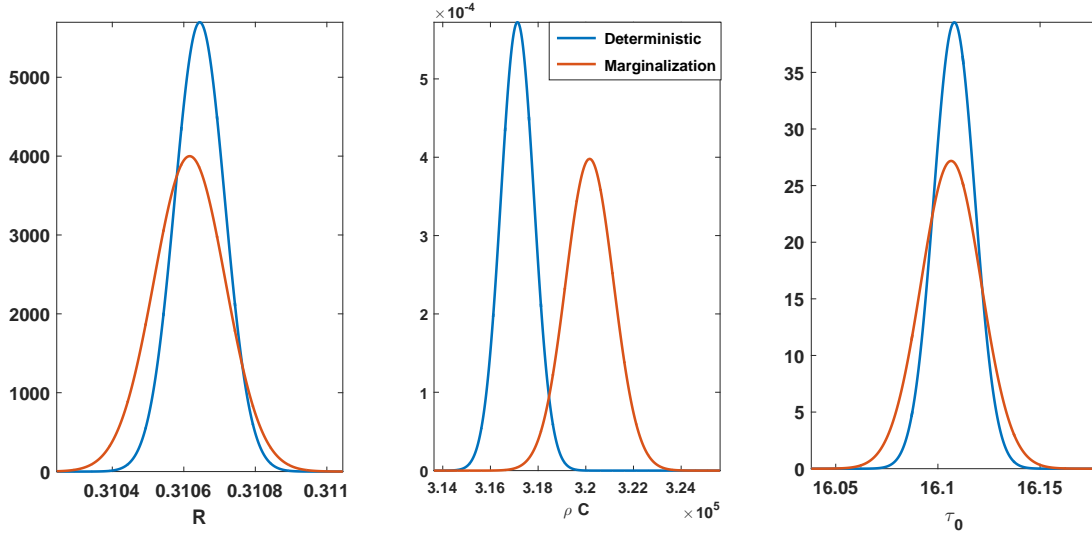


Figure 16: Comparison between the marginal posteriors obtained by the deterministic approach (Figure 8) and the marginalization approach (Figure 13).

compare the variability between drawing 4 and 3 observations. Clearly, the uncertainty increases when small subsamples are used. Similarly, Figure 18 shows the difference in variability between sampling algorithms that randomly draw 8, 7 and 6 observations from each subinterval. In general, the variability intervals include our MAP estimate of θ obtained in Example 3.4. These intervals are within a reasonable range. Such results ensure the robustness of our Bayesian methodology in estimating the thermal properties of a wall.

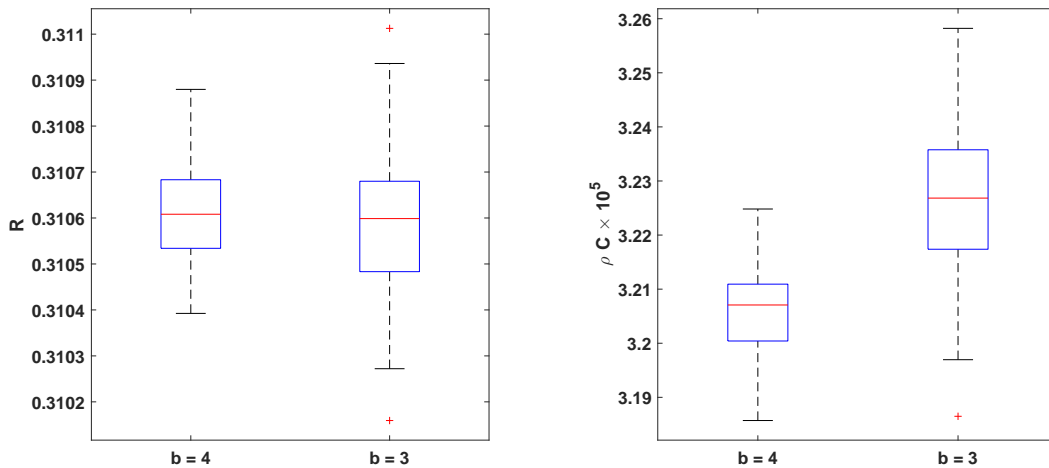


Figure 17: The variability of R and ρC using subsampling algorithms with subinterval length $\ell = 5$ and subsample sizes $b = 4$ and 3 .

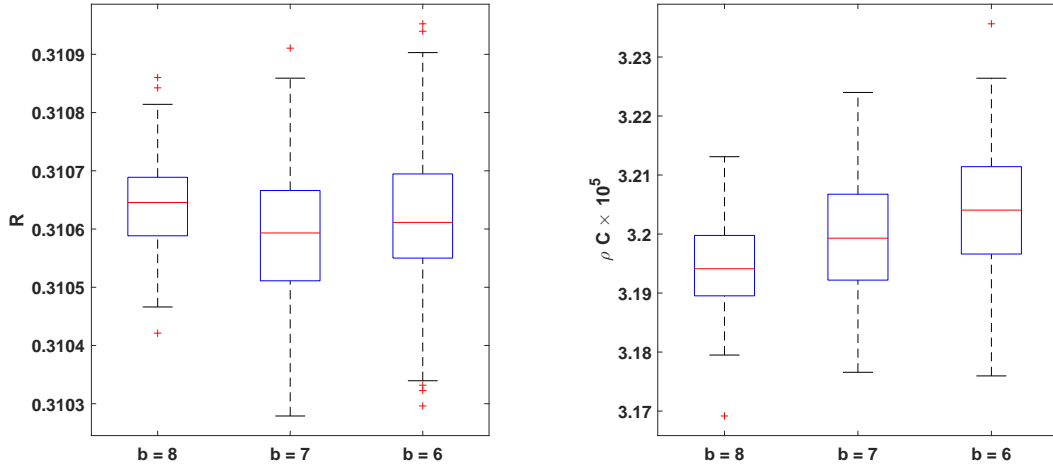


Figure 18: The variability of R and ρC using subsampling algorithms with subinterval length $\ell = 10$ and subsample sizes $b = 8, 7$ and 6 .

4. Information gain

In a Bayesian framework, the utility of an experiment can be measured by the so-called information gain (relative entropy) function, which is defined by the Kullback-Leibler divergence between the prior density function, $\rho_p(\theta)$, and the posterior density function, $\rho(\theta|\mathbf{Q}_{int}, \mathbf{Q}_{ext}, \xi)$:

$$D_{KL}(\mathbf{Q}_{int}, \mathbf{Q}_{ext}, \xi) := \int_{\Theta} \log \left(\frac{\rho(\theta|\mathbf{Q}_{int}, \mathbf{Q}_{ext}, \xi)}{\rho_p(\theta)} \right) \rho(\theta|\mathbf{Y}, \xi) d\theta, \quad (11)$$

where ξ is the experimental setup [13, 14].

We first consider an experimental setup that describes the duration of the measurement campaign. We use the Laplace approximation to compute the information gain for overlapping increasing time intervals. Figure 19 and Table 1 summarize the computations. As expected, the information gain increases over time as more observations are incorporated into the Bayesian inference. However, we observe that after 5000 minutes, the rate of increase of the information gain slows, indicating that the collected measurements provide reliable information on the thermal properties of the solid brick wall. We introduce another experimental setup by considering the external temperature oscillation. Figure 20 shows how data are partitioned on the basis of the detected external temperature cycles in Room 2. We estimate the information gain for each cycle and the results are summarized in Table 2. Cycles 1 and 3 are ranked as the most informative in terms of the Kullback-Leibler divergence, while Cycle 2 is the least informative, although Cycle 4 has the shortest duration. From these results, we can deduce that larger temperature oscillations bring more knowledge to the inference about θ , suggesting that steady state conditions cannot be used to infer the thermal properties of the wall.

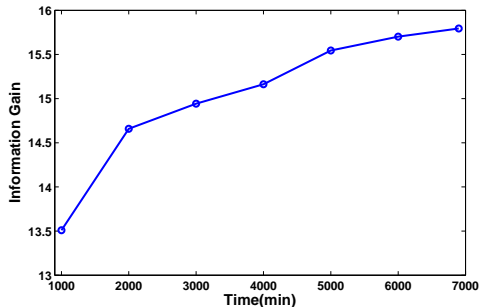


Figure 19: The estimated information gain with respect to time.

Time (min)	D_{KL}
1000	13.51
2000	14.66
3000	14.94
4000	15.16
5000	15.55
6000	15.70
6900	15.79

Table 1: The estimated information gain over time.

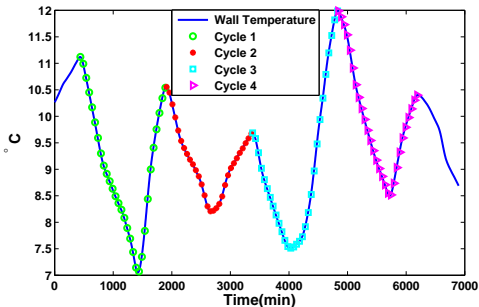


Figure 20: Different temperature cycles.

Cycle	Time (min)	D_{KL}
1	1470	14.46
2	1470	13.68
3	1460	14.47
4	1370	13.98

Table 2: The estimated information gain from the detected external temperature oscillation cycles.

5. Summary and conclusions

Our goal is to advance the mathematical modeling of the thermal properties of walls through statistical inference when in-situ measurements of surface temperatures and heat flux are available. Existing approaches are based on simplified models [9]. Our approach uses the heat equation as a forward model to describe the heat dynamics of the wall. Moreover, our statistical methodology uses a marginalization technique that includes uncertainty in the temperature measurements, which are often incorporated as exact readings. We are thus able to achieve high error reduction and remove the bias due to the measurement error in the boundary temperature readings. Experimental data collected under controlled conditions demonstrate the utility of our method. To reduce the noise inherent in the experimental data, we smooth the temperature and heat flux time series with a local averaging procedure, whose bandwidth is chosen to ensure the minimization of the autocorrelation function.

We considered two main numerical examples. In the first example, we explored a deterministic approach in which where smoothed temperature measurements are used as exact boundary conditions. In the second example, we removed this deterministic constraint by modeling the nuisance boundary conditions as Gaussian random functions that are then marginalized analytically. In both examples, we derived the ML estimates of the thermal properties of the wall and the approximated posterior densities of such parameters by the Laplace method and the random-walk Metropolis-Hastings algorithm. We remark that, in both examples, the two techniques for the approximated Bayesian inference produce similar marginal posterior densities for the physical parameters of the wall. We emphasize that our numerical results show that the use of the marginalization technique considerably reduces the bias error of the estimates of the model parameters, in contrast to when boundary conditions are assumed to be deterministic. Moreover, our estimates of the thermal resistance and the heat capacitance of the wall are consistent with the corresponding tabulated values for the wall under examination [17]. We carried out computationally

intensive experiments to analyze the convergence of the MAP estimates, which are computed with the numerical solver when the space step, Δx , and the time step, Δt , are small. In addition, we have checked the robustness of our Bayesian inference framework in estimating parameters of the heat equation model, using the design and the application of subsampling algorithms with different subinterval lengths and subsample sizes.

Finally, in the Bayesian framework, we have estimated the information gain when the experimental setup consists either of the duration of the measurement campaign or the amplitude of the external temperature oscillation cycle. In this way, we can make recommendations on how to plan an efficient experimental design. Our numerical results indicate that a period of about 3.5 days is sufficient to gather data that allow the physical parameters of interest to be inferred with a high degree of accuracy. Moreover, our analysis shows that data corresponding to the oscillation cycles, which are characterized by a large variation in the temperature range are informative. Our approach allows us to determine the optimal duration of the measurement campaign and the temperature oscillation cycle, both of which are important to practitioners. Indeed, standard methods have required that data should be collected for two weeks, during the winter, such that high oscillations in temperature be avoided [11]. The numerical examples reported in this work, applied to experimental data, indicate that our approach provides an accurate and robust methodology for inferring the thermal properties of solid brick walls, as well as for determining optimal experimental conditions for cost-effective measurement campaigns.

Acknowledgements

Part of this work was carried out while M. Iglesias and M. Scavino were Visiting Professors at KAUST. Z. Sawlan, M. Scavino and R. Tempone are members of the KAUST SRI Center for Uncertainty Quantification in Computational Science and Engineering. R. Tempone received support from the KAUST CRG3 Award Ref: 2281.

References

References

- [1] United Nations, Status of ratification of the Kyoto protocol, “http://unfccc.int/kyoto_protocol/status_of_ratification/items/2613.php” (October 2014).
- [2] Climate Change Act 2008, Chapter 27, Act of the Parliament of the United Kingdom. URL “http://www.legislation.gov.uk/ukpga/2008/27/pdfs/ukpga_20080027_en.pdf”
- [3] International Energy Agency, Energy efficiency, <http://www.iea.org/aboutus/faqs/energyefficiency/> (2016).
- [4] S. H. Hong, T. Oreszczyn, I. Ridley, The impact of energy efficient refurbishment on the space heating fuel consumption in English dwellings, *Energy and Buildings* 38 (10) (2006) 1171–1181.
- [5] P. G. Cesaratto, M. De Carli, A measuring campaign of thermal conductance in situ and possible impacts on net energy demand in buildings, *Energy and Buildings* 59 (2013) 29–36.
- [6] F. Asdrubali, F. D’Alessandro, G. Baldinelli, F. Bianchi, Evaluating in situ thermal transmittance of green buildings masonries—A case study, *Case Studies in Construction Materials* 1 (2014) 53–59.
- [7] F. G. Li, A. Z. P. Smith, P. Biddulph, I. G. Hamilton, R. Lowe, A. Mavrogianni, E. Oikonomou, R. Raslan, S. Stamp, A. Stone, et al., Solid-wall U-values: heat flux measurements compared with standard assumptions, *Building Research & Information* 43 (2) (2015) 238–252.

- [8] S. de Wit, Uncertainty in building simulation, in: A. M. Malkawi, G. Augenbroe (Eds.), *Advanced Building Simulation*.
- [9] P. Biddulph, V. Gori, C. A. Elwell, C. Scott, C. Rye, R. Lowe, T. Oreszczyn, Inferring the thermal resistance and effective thermal mass of a wall using frequent temperature and heat flux measurements, *Energy and Buildings* 78 (2014) 10–16.
- [10] C. Luo, B. Moghtaderi, S. Hands, A. Page, Determining the thermal capacitance, conductivity and the convective heat transfer coefficient of a brick wall by annually monitored temperatures and total heat fluxes, *Energy and Buildings* 43 (2–3) (2011) 379–385.
- [11] ISO 9869-1:2014, Thermal insulation - building elements - in-situ thermal resistance and thermal transmittance - part 1: Heat flow meter method, Tech. rep., The British Standards Institution (2014).
- [12] O. Gutschker, Parameter identification with the software package LORD, *Building and Environment* 43 (2) (2008) 163–169.
- [13] S. Kullback, R. A. Leibler, On information and sufficiency, *The Annals of Mathematical Statistics* 22 (1) (1951) 79–86.
- [14] Q. Long, M. Scavino, R. Tempone, S. Wang, Fast estimation of expected information gains for Bayesian experimental designs based on Laplace approximations, *Computer Methods in Applied Mechanics and Engineering* 259 (1) (2013) 24–39.
- [15] F. Ruggeri, Z. Sawlan, M. Scavino, R. Tempone, A hierarchical Bayesian setting for an inverse problem in linear parabolic PDEs with noisy boundary conditions, *Bayesian Analysis* doi:10.1214/16-BA1007.
- [16] D. Sivia, J. Skilling, *Data analysis: a Bayesian tutorial*, Oxford University Press, 2006.
- [17] CIBSE, *Guide A: Environmental design*, The Chartered Institution of Building Services Engineers, London.
- [18] P. Craven, G. Wahba, Smoothing noisy data with spline functions, *Numerische Mathematik* 31 (4) (1978) 377–403.
- [19] C. M. Hurvich, J. S. Simonoff, C.-L. Tsai, Smoothing parameter selection in nonparametric regression using an improved Akaike information criterion, *Journal of the Royal Statistical Society: Series B (Statistical Methodology)* 60 (2) (1998) 271–293.
- [20] J. K. Ghosh, M. Delampady, T. Samanta, *An Introduction to Bayesian Analysis: theory and methods*, Springer, 2006.
- [21] C. P. Robert, G. Casella, *Introducing Monte Carlo Methods with R*, Springer, 2009.

6. Appendix

6.1. Proof of Theorem 2.1

Proof. Let us introduce the following notation: $T_{m,n} = T(m\Delta x, n\Delta t)$, $T_{int}(n\Delta t) = T_{int,n}$ and $T_{ext}(n\Delta t) = T_{ext,n}$. The backward Euler discretization of the heat equation in the interval, $(n\Delta t, (n+1)\Delta t)$, is given by

$$\begin{cases} \frac{1}{\Delta t}(T_{m,n+1} - T_{m,n}) - \frac{\eta}{\Delta x^2}(T_{m+1,n+1} - 2T_{m,n+1} + T_{m-1,n+1}) = 0, & m = 1, \dots, M-1 \\ T_{0,n+1} = T_{int,n+1}, \\ T_{M,n+1} = T_{ext,n+1}, \end{cases} \quad (12)$$

where $\eta = \frac{k}{\rho C}$.

Let us introduce the vectors $\mathbf{T}_n = (T_{1,n}, \dots, T_{M-1,n})'$, $n = 0, \dots, N$, and the matrix

$$\mathbf{A}_{(M-1) \times (I-1)} = \begin{pmatrix} -2 & 1 & 0 & 0 & \dots & 0 \\ 1 & -2 & 1 & 0 & \dots & 0 \\ 0 & 1 & -2 & 1 & \dots & 0 \\ \vdots & \ddots & \ddots & \ddots & \ddots & \vdots \\ 0 & \dots & 0 & 1 & -2 & 1 \\ 0 & 0 & 0 & \dots & 1 & -2 \end{pmatrix}.$$

The discretized system (12) can be written in a matrix form as

$$\frac{1}{\Delta t}(\mathbf{T}_{n+1} - \mathbf{T}_n) - \frac{\eta}{\Delta x^2} \mathbf{A} \mathbf{T}_{n+1} = \frac{\eta}{\Delta x^2} (T_{int,n+1} \mathbf{a} + T_{ext,n+1} \mathbf{b}), \quad (13)$$

where $\mathbf{a}_{(M-1) \times 1} = (1, 0, \dots, 0)'$, $\mathbf{b}_{(M-1) \times 1} = (0, \dots, 0, 1)'$.

The expression (13) is equal to

$$(I_{I-1} - \eta \frac{\Delta t}{\Delta x^2} \mathbf{A}) \mathbf{T}_{n+1} = \mathbf{T}_n + \eta \frac{\Delta t}{\Delta x^2} (T_{int,n+1} \mathbf{a} + T_{ext,n+1} \mathbf{b}).$$

By letting $\frac{\Delta t}{\Delta x^2} = \lambda$ and $\mathbf{B} = (I_{M-1} - \eta \lambda \mathbf{A})^{-1}$, we obtain

$$\mathbf{T}_{n+1} = \mathbf{B} \mathbf{T}_n + \eta \lambda (T_{int,n+1} \mathbf{B} \mathbf{a} + T_{ext,n+1} \mathbf{B} \mathbf{b}).$$

Applying recursively the previous relation, we derive

$$\mathbf{T}_n = \mathbf{B}^n \mathbf{T}_0 + \eta \lambda \sum_{k=1}^n T_{int,k} \mathbf{B}^{n-k+1} \mathbf{a} + \eta \lambda \sum_{k=1}^n T_{ext,k} \mathbf{B}^{n-k+1} \mathbf{b}.$$

Now, we approximate F_{int} and F_{ext} using forward and backward differences with second-order error:

$$F_{int}(t_n) \approx \frac{k}{2\Delta x} (3T_{int,n} - 4T_{1,n} + T_{2,n}), \quad (14)$$

$$F_{ext}(t_n) \approx \frac{k}{2\Delta x} (3T_{ext,n} - 4T_{M-1,n} + T_{M-2,n}). \quad (15)$$

By defining the vectors $\mathbf{c}_{(M-1) \times 1} = (-4, 1, 0, \dots, 0)'$ and $\mathbf{d}_{(M-1) \times 1} = (0, \dots, 0, 1, -4)'$, we obtain

$$F_{int}(t_n) \approx \frac{k}{2\Delta x} \left[\mathbf{c}' \mathbf{B}^n \mathbf{T}_0 + 3T_{int,n} + \eta \lambda \sum_{k=1}^n T_{int,k} \mathbf{c}' \mathbf{B}^{n-k+1} \mathbf{a} + \eta \lambda \sum_{k=1}^n T_{ext,k} \mathbf{c}' \mathbf{B}^{n-k+1} \mathbf{b} \right],$$

$$F_{ext}(t_n) \approx \frac{k}{2\Delta x} \left[\mathbf{d}' \mathbf{B}^n \mathbf{T}_0 + \eta \lambda \sum_{k=1}^n T_{int,k} \mathbf{d}' \mathbf{B}^{n-k+1} \mathbf{a} + 3T_{ext,n} + \eta \lambda \sum_{k=1}^n T_{ext,k} \mathbf{d}' \mathbf{B}^{n-k+1} \mathbf{b} \right].$$

Finally, we construct the matrices $H_{(N+1) \times (M-1)}$, $H_{int}_{(N+1) \times (N+1)}$ and $H_{ext}_{(N+1) \times (N+1)}$ as follows:

- the matrix H has the row vectors $H^i = \frac{k}{2\Delta x} \mathbf{c}' \mathbf{B}^{i-1}$, $i = 1, \dots, N+1$;

- the matrix H_{int} is lower triangular and is given by

$$\frac{k\eta\lambda}{2\Delta x} \begin{bmatrix} \frac{3}{\eta\lambda} & 0 & 0 & \dots & 0 \\ 0 & \frac{3}{\eta\lambda} + \mathbf{c}'\mathbf{B}\mathbf{a} & 0 & \dots & 0 \\ 0 & \mathbf{c}'\mathbf{B}^2\mathbf{a} & \frac{3}{\eta\lambda} + \mathbf{c}'\mathbf{B}\mathbf{a} & \dots & 0 \\ \vdots & \vdots & \vdots & \ddots & \vdots \\ 0 & \mathbf{c}'\mathbf{B}^N\mathbf{a} & \mathbf{c}'\mathbf{B}^{N-1}\mathbf{a} & \dots & \frac{3}{\eta\lambda} + \mathbf{c}'\mathbf{B}\mathbf{a} \end{bmatrix};$$

- the matrix H_{ext} is lower triangular and is given by

$$\frac{k\eta\lambda}{2\Delta x} \begin{bmatrix} 0 & 0 & 0 & \dots & 0 \\ 0 & \mathbf{c}'\mathbf{B}\mathbf{b} & 0 & \dots & 0 \\ 0 & \mathbf{c}'\mathbf{B}^2\mathbf{b} & \frac{3}{\eta\lambda} + \mathbf{c}'\mathbf{B}\mathbf{b} & \dots & 0 \\ \vdots & \vdots & \vdots & \ddots & \vdots \\ 0 & \mathbf{c}'\mathbf{B}^N\mathbf{b} & \mathbf{c}'\mathbf{B}^{N-1}\mathbf{b} & \dots & \mathbf{c}'\mathbf{B}\mathbf{b} \end{bmatrix}.$$

Similarly, we can construct the matrices $G_{(N+1)\times(M-1)}$, $G_{int (N+1)\times(N+1)}$ and $G_{ext (N+1)\times(N+1)}$.

□